

10-28-1991

Microscopy of Mixed Surfaces on Layered Semiconductors

L. Margulis

Weizmann Institute of Science

D. Mahalu

Weizmann Institute of Science

B. Parkinson

DuPont R&D Department

R. Tenne

Weizmann Institute of Science

Follow this and additional works at: <https://digitalcommons.usu.edu/microscopy>



Part of the [Biology Commons](#)

Recommended Citation

Margulis, L.; Mahalu, D.; Parkinson, B.; and Tenne, R. (1991) "Microscopy of Mixed Surfaces on Layered Semiconductors," *Scanning Microscopy*. Vol. 5 : No. 4 , Article 6.

Available at: <https://digitalcommons.usu.edu/microscopy/vol5/iss4/6>

This Article is brought to you for free and open access by the Western Dairy Center at DigitalCommons@USU. It has been accepted for inclusion in Scanning Microscopy by an authorized administrator of DigitalCommons@USU. For more information, please contact digitalcommons@usu.edu.



MICROSCOPY OF MIXED SURFACES ON LAYERED SEMICONDUCTORS

L. Margulis*, D. Mahalu, B. Parkinson† and R. Tenne

Department of Materials Research, Weizmann Institute of Science, Rehovot 76100, Israel

† DuPont R & D Department, Experimental Station, Wilmington, DE 19898, USA

(Received for publication May 6, 1991, and in revised form October 28, 1991)

Abstract

A large number of well-defined hexagonal etch pits is produced on the WSe₂ surface by controlled anisotropic corrosion. As a result a **mixed** surface (combining both $\perp c$ and $\parallel c$ components) is created. This surface exhibits photovoltaic properties even better than the atomically smooth van der Waals surface. Measurements of electron beam induced current performed at low temperatures give direct evidence for enhanced current collection of $\parallel c$ facets. Observations made by transmission electron microscopy and scanning tunneling microscopy show the presence of very low $\parallel c$ steps on the van der Waals surface.

Introduction

Semiconductor/electrolyte interfaces started to be intensively studied some thirty years ago when scientists trained both in solid state physics and electrochemistry realized that interfacial problems in electronic junctions can be handled easier when a liquid junction is used. One of the key advantages of semiconductor/liquid junctions is the ability to access the surface junction under operating cell conditions and to perform in-situ chemical treatments which can improve the junction behavior. Some chemical methods have been shown to be extremely effective in improving the performance of certain semiconductor/liquid or semiconductor/metal junctions (Heller 1981).

As stated before (Heller 1981, Hodes et al. 1985), interfacial problems in semiconductor/electrolyte systems involved in photovoltaic devices are difficult to control and they usually dominate the electronic behavior of the device. The problem is even more complicated when anisotropic semiconductors, exposing different crystallographic facets, are used. Due to the anisotropy of the material, preferential photon absorption on specific facets or preferential carrier collection on others can be expected. On the other hand, contact problems connected with anisotropic exposure of intrinsic surface states must be also considered. Such a complex situation is known to occur when Schottky junctions between VIa-VIb layered semiconductors, e.g. WSe₂, and suitable electrolyte, like I₂/KI (or metals as Au), are to be obtained (Kautek et al. 1980).

WSe₂ is a semiconductor which is very suitable for both Schottky and liquid junction photovoltaic cells due to its high absorption coefficient of sunlight and its excellent chemical stability in air and liquid media (Tributsch 1978, Lewerenz et al. 1980).

The hexagonal crystal lattice of WSe₂ is built by periodic stacking of triple atomic layers Se-W-Se in the c-direction, with weak van der Waals (vdW) bonds between Se-layers. Consequently, WSe₂ is characterized by

Key Words: Layered semiconductors, WSe₂, EBIC, electron microscopy, photovoltaics, mixed surface

*Address for correspondence:

Lev M. Margulis
Department of Materials Research, Weizmann Institute of Science, Rehovot 76100, Israel.

Phone No. (972)-8-343504

strong anisotropy of its electronic and mechanical properties (Wilson and Yoffe 1969) in mutually orthogonal ($\parallel c$ and $\perp c$) crystallographic directions. The WSe_2 crystal can be easily cleaved along the vdW ($\perp c$) planes exposing an atomically smooth Se surface. It was generally accepted that the collection efficiency of minority carriers, and hence light to electricity conversion efficiency of those crystals, depends on the quality of the exposed vdW surface. The charge carrier collection deficiency was usually associated with electrically active defects such as $\parallel c$ surface steps and near-surface dislocations (Kam and Parkinson 1982, Lewerenz et al. 1982).

Controlled anisotropic corrosion (CAC) was found earlier (Mahalu et al. 1990) to be a successful method of chemical preparation of a **mixed** surface on WSe_2 . It was shown that as a result of CAC the existing surface states are entirely passivated, and a complex geometrical structure which involves, in a cooperative manner, both $\perp c$ and $\parallel c$ facets is formed. Such a structure was found to be a **photoactive mixed surface** (Mahalu et al. 1991, Phys. Rev. B, accepted for publication). It exhibits unitary quantum efficiency (in the maximum absorption range of the material) over extended areas together with other unique optoelectronic properties.

The purpose of this paper was to characterize the morphology of the mixed surface by high resolution microscopic techniques and to make a direct comparison of the current collection efficiencies of the two main components of the mixed surface, i.e. $\perp c$ and $\parallel c$ facets.

Materials and Methods

Single crystals of n-type WSe_2 were grown by chemical vapor transport with bromine as the transport agent. The crystals were approximately 0.3 mm thick with surface areas between 0.2 and 0.8 cm². CAC was used to obtain mixed surfaces on freshly cleaved WSe_2 crystals (Mahalu et al. 1990). For this purpose the crystals were provided with ohmic contacts by first rubbing with an indium-gallium alloy; they were then attached to a titanium substrate and encapsulated with an insulating epoxy. Since the smooth, defect free vdW surface of n- WSe_2 is inert towards oxidation, corrosion and anodic decomposition (Jaegermann and Schmeisser 1986, Mahalu et al. 1990), dislocations which serve as nucleation sites for the CAC process were deliberately introduced by mechanical indentation. CAC was carried out in 1M HCl solution, using a classical three-electrode potentiostatic arrangement with a Pt electrode as a reference. Finally the samples were carefully rinsed and soaked in hot (60°C) 2M KOH solution to remove insoluble WO_3 and occluded selenium oxide.

Secondary electron (SE) and electron beam induced current (EBIC) images were obtained using a Philips 515 scanning electron microscope (SEM) equipped with

a Hexland cold stage, at temperatures between 115 and 300 K. The accelerating voltage was varied between 20 and 30 kV. Schottky barriers were fabricated by evaporation of a 250 Å thick gold layer. The gold was evaporated at an angle of 45° in order to provide equal thickness of the Schottky contacts on $\parallel c$ and $\perp c$ facets, at least for a certain part of the etch pit area. For increasing the signal/noise ratio, the Schottky contact areas were considerably restricted, in the range 100 to 300 μm in diameter. The electrical connection to the Schottky contacts was realized using an electrolytically sharpened gold needle (see Fig. 4). The comparative EBIC measurements were performed at 45°-tilted position. Thus an identical orientation of $\parallel c$ and $\perp c$ facets relative to the electron beam was ensured.

For transmission electron microscopy (TEM) a Philips 400T microscope was used. Thin foils for TEM studies were prepared from the etched crystals by cleavage. Very careful cleavage was needed in order to get foils with large enough areas transparent to 120 kV electrons. Scanning tunneling microscopy (STM) of freshly cleaved and CAC etched WSe_2 surface was performed using a Nanoscope II (Digital Instruments).

Results

Morphology of the mixed surface on microscale

Morphological characterization of the mixed surface (with resolution up to a few microns) was done previously by Mahalu et al. (1988) and Jakubowicz et al. (1989). One of the purposes of this work was to describe more precisely the morphology of etch pits obtained on the WSe_2 surface as a result of the CAC process. A general view of the mixed surface created after CAC is shown in Fig. 1. This surface is characterized by the presence of well-defined hexagonal etch pits and individual $\parallel c$ steps in the regions between these pits. The typical depth of the etch pits is ca. 20 μm while the height of individual $\parallel c$ steps resolvable in the scanning electron images varied between 0.1 and 0.5 μm, as it was determined by measuring step projections at 45°-tilted position.

Further information about the morphology of the mixed surface was obtained by use of STM and TEM techniques which provide better lateral and depth resolution than SEM. We could learn from STM images that even large regions of the mixed surface that appeared to be as smooth as cleaved vdW planes in SEM (like area S in Fig. 1), are actually composed of very low (~ 50 Å) $\parallel c$ steps (Fig. 2b). The average distance between these steps is of about 500 Å.

TEM observations are in excellent agreement with STM data. One can clearly see in TEM image of the mixed surface (Fig. 3a) that the distance between the steps is 400 - 500 Å. These are $\parallel c$ steps because the corresponding convergent beam electron diffraction (CBED)

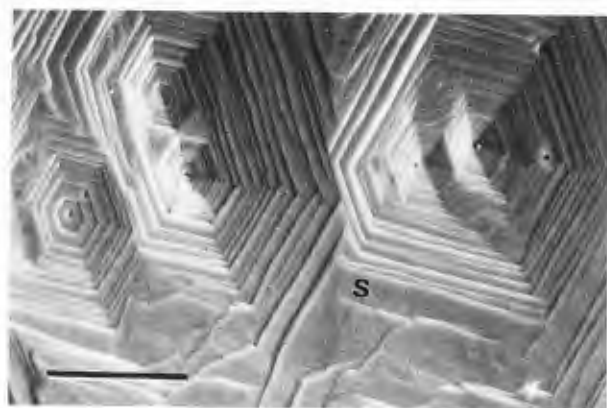


Figure 1. SE image of the mixed surface of WSe_2 single crystal. The regular shape of the hexagonal etch pits is slightly distorted because of the 45° -tilt. Bar is $20 \mu m$.

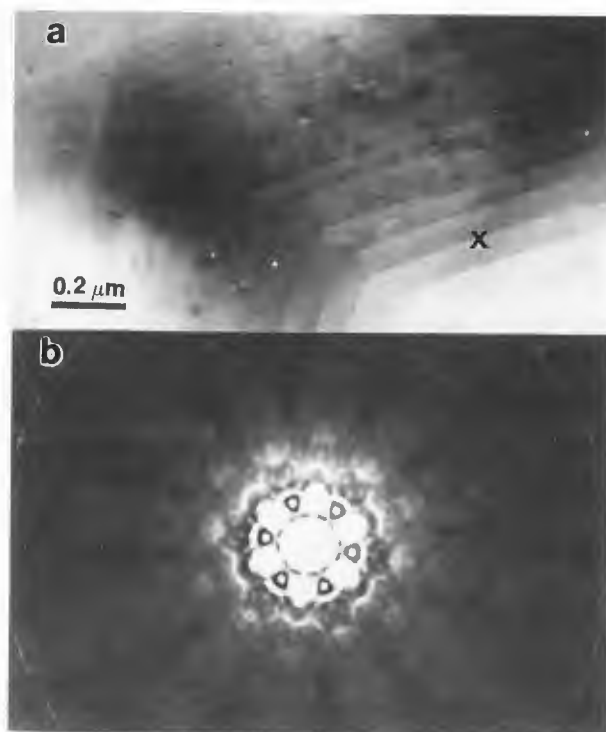


Figure 3. TEM micrograph of an area of the mixed surface (a) and CBED pattern (b) taken at point x . Note well-defined six-fold symmetry of CBED pattern proving high perfection of the crystal.

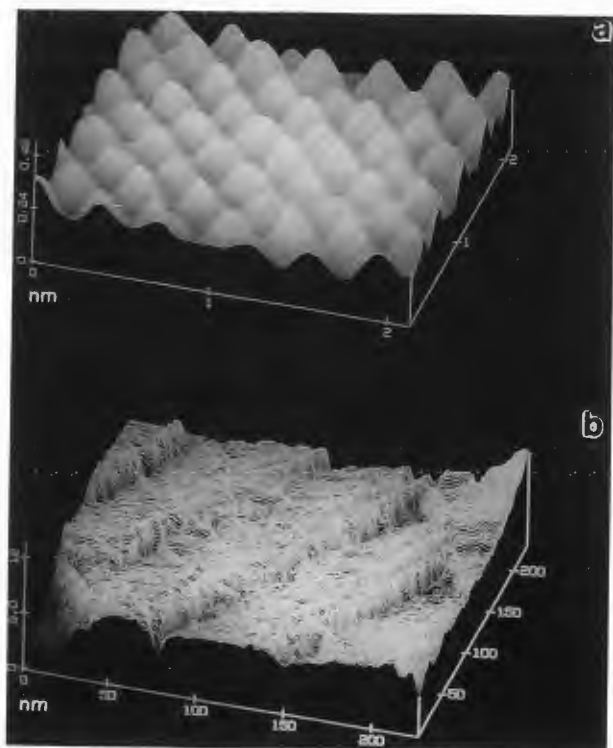


Figure 2. STM micrographs of the perfect region of smooth vdW surface (a) and the mixed surface created after CAC (b).

pattern shows that the c -axis is exactly parallel to the incident electron beam (Fig. 3b). It is quite difficult to measure the height of these steps but some estimations (based on a calculation of number of steps per extinction length) give evidence that it must be about $30 - 40 \text{ \AA}$, i.e. again in a good correlation with STM observations.

EBIC comparative measurements

It was already clear from the previous measurements that an unusual geometry of the crystal surface was designed, using CAC. The goal of the EBIC experiments was the direct comparison of the current collection efficiency of $\parallel c$ and $\perp c$ components of the mixed surface. Such a comparison was not made earlier (Mahalu et al. 1988, Jakubowicz et al. 1989) because of experimental difficulties: since the EBIC signal from the Au/WSe_2 Schottky diodes was rather weak at room temperature, high beam currents (i.e. large spot sizes, of at least $0.2 \mu m$), had to be used in order to obtain a proper signal. Under these conditions, good spatial resolution cannot be expected. Furthermore, severe electron damage is observed even after the first scan. Therefore observations at high magnification are practically impossible at room temperature.

It was found that this problem can be avoided by lowering the sample temperature. Cooling the WSe_2 crystal prevents almost totally the electron beam damage and simultaneously results in remarkable enhancement of the EBIC signal. Using low temperatures ($115 - 180 \text{ K}$) enabled to obtain EBIC images of even very low $\parallel c$ steps (Fig. 4 - 7).

An enhancement of the EBIC can be detected in the vicinity of $\parallel c$ facets even if the crystal surface is in a horizontal position, and the electron beam glides along $\parallel c$ facets (Fig. 4b). In this orientation, ridges formed by the intersection of $\parallel c$ and $\perp c$ facets are transparent for primary electrons; therefore the EBIC signal is noticeably reduced at these ridges, and the EBIC contrast appears as bright/dark/bright. The difference in the EBIC signals for $\parallel c$ and $\perp c$ facets is revealed more distinctly when the crystal is tilted by 45° (Fig. 5b). In this latter case the enhanced EBIC signal for $\parallel c$ facets is clearly seen on the left side of the etch pit where $\parallel c$ and $\perp c$ facets form equal angles (45°) with the electron beam. On the right side of the etch pit the situation is quite different. The $\parallel c$ facets appear here with dark contrast due to two reasons. First, they are shadowed by $\perp c$ components. Second, the primary electrons can be transmitted through the corners, formed by $\parallel c$ and $\perp c$ facets without high energy losses, and hence the concentration of electron-hole pairs is noticeably lower at the corners than in the bulk. The dark EBIC contrast that resulted from near-surface defects appears also in some areas inside the etch pit.

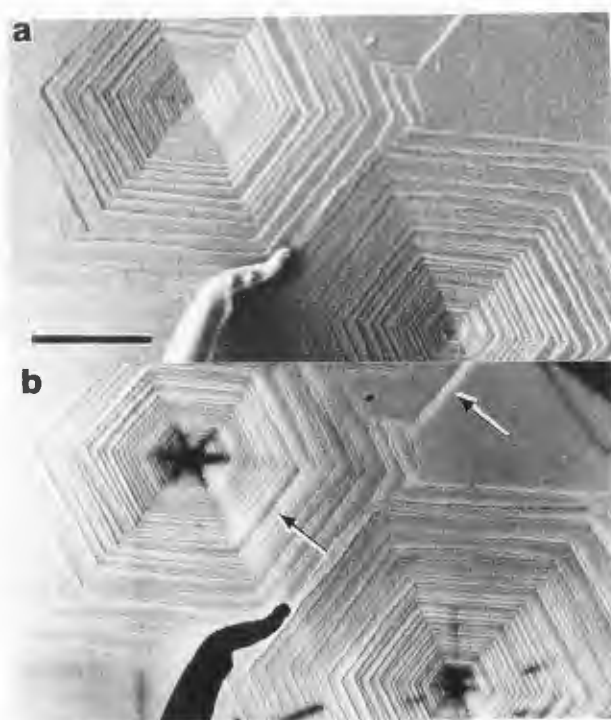


Figure 4. SE (a) and EBIC (b) images of two large etch pits taken for the specimen in the horizontal position. Note enhanced EBIC signal in the vicinity of $\parallel c$ steps (arrowed). One can also see the gold needle that serves as an electrical contact and dislocations (b) which give very strong contrast when they come nearer to the surface. The specimen temperature is 120 K. Bar is 50 μm .

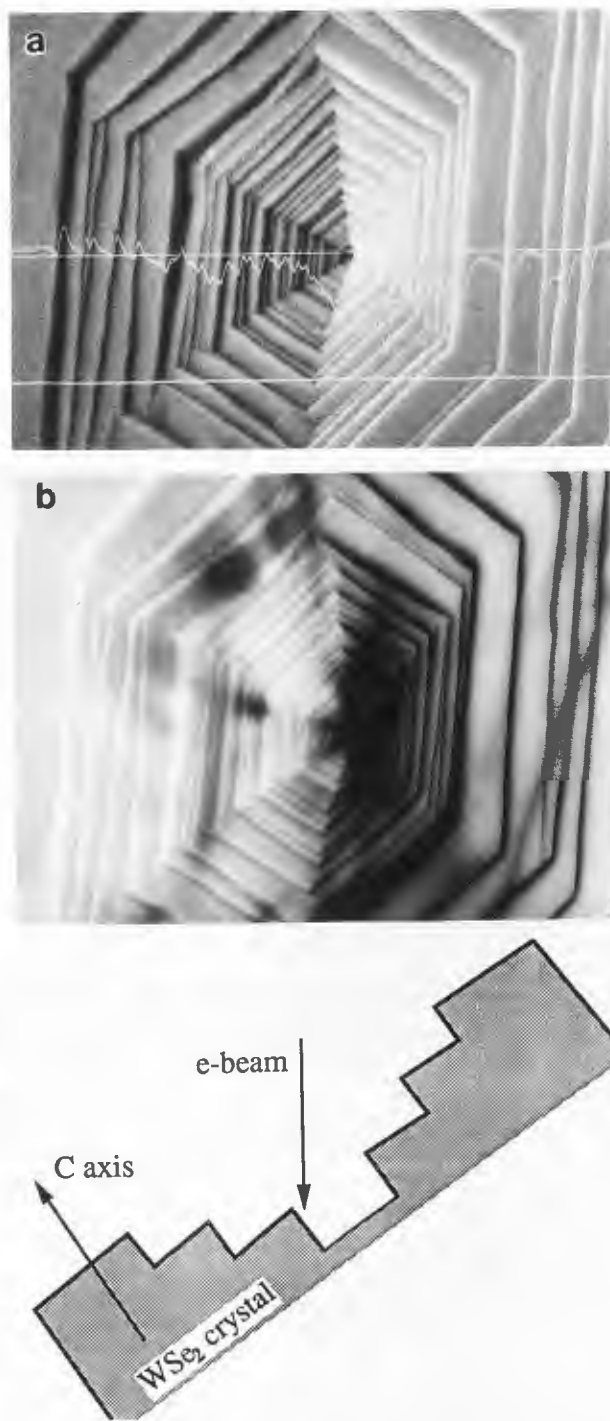


Figure 5. SE (a) and EBIC (b) images of an etch pit taken for the specimen in tilted (45°) position as shows the scheme at the bottom. Three profiles are superimposed on the SE picture: EBIC zero (lower horizontal line), line scan (upper horizontal line) and EBIC signal profile. Local enhancement of the EBIC signal on $\parallel c$ facets is clearly seen. The specimen temperature is 120 K. Bar is 50 μm .

The comparative measurements of the EBIC for $\parallel c$ and $\perp c$ facets (see EBIC signal profiles in Fig. 5 and 6) show that $\parallel c$ facets provide remarkably higher current collection efficiency. The EBIC signal enhancement at these facets equals ca. 20% (at least for big enough facets) independent of the accelerating voltage and temperature. This effect can be clearly seen in Fig. 6.

Fig. 7 shows an interesting image of an WSe_2 surface at an initial stage of CAC. One can see here, as earlier, an enhanced EBIC signal on the $\parallel c$ steps. At the same time a diminished EBIC signal (strong black contrast) can be observed along $\parallel c$ steps at loci (Fig. 7b, arrowed) where the process of recombination site passivation is still not finished. This observation serves as an additional proof for the efficiency of the EBIC technique for evaluation of the photoresponse of local surface features. Black EBIC contrast (enhanced carrier recombination) appears also in Fig. 7b at the dislocation line and near-surface spot defect.

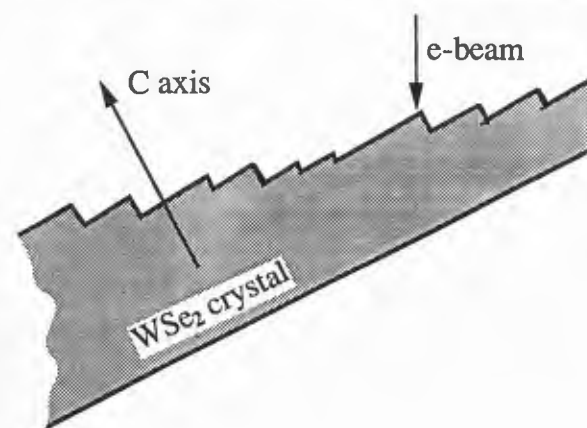
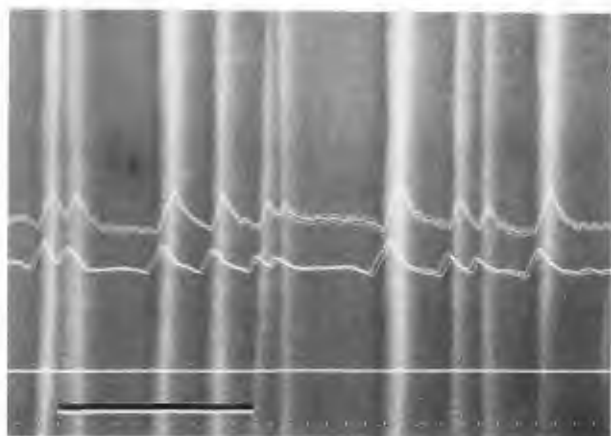


Figure 6. EBIC image of $\parallel c$ facets and EBIC profiles for 150 and 180 K (upper and lower curves respectively). The crystal is tilted by 45° . EBIC zero line is also shown. It coincides with line scan. Bar is $10 \mu\text{m}$.

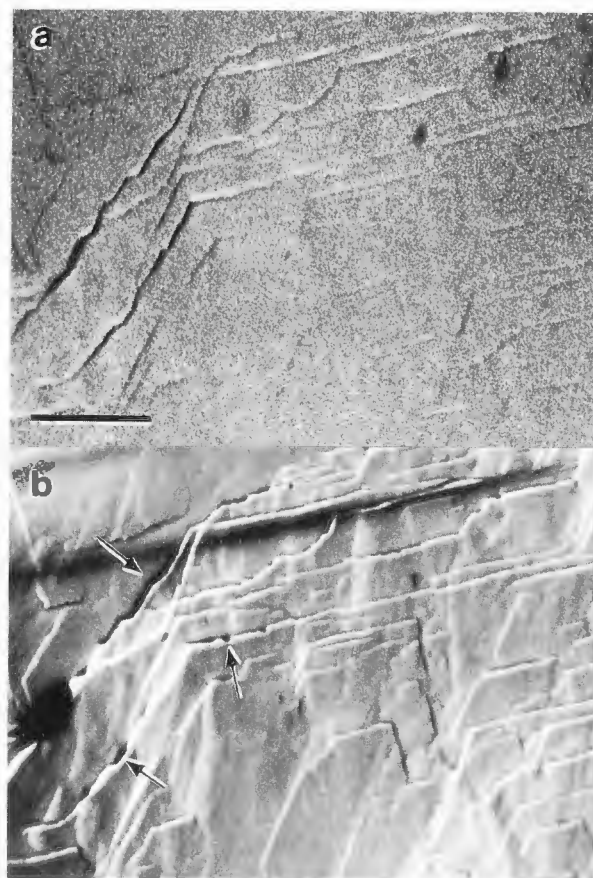


Figure 7. SE (a) and EBIC (b) images of the mixed surface at initial stage of CAC. The crystal is tilted by 45° . The specimen temperature is 130 K. Bar is $20 \mu\text{m}$. See text for further explanation.

Conclusion

The results obtained in this study allow us to conclude that CAC yields unique surface morphology on both the macro- and microscopic scales. This surface includes new elements - $\parallel c$ facets - which reveal enhanced current collection in comparison with vdW surface. This phenomenon may have special applications in optoelectronics, and it needs further investigation.

Acknowledgements

This research was supported by grants from the Israel National Council for Research and Development and the KFA Jülich (Germany). L.M. thanks the Israel Ministry of Science for partial support. The authors are grateful to A Jakubowicz and R Matson for helpful discussions and to A Wold for providing part of the crystals. The authors also wish to thank J Meakin for revising the manuscript.

References

- Heller A (1981) Conversion of Sunlight into Electrical Power and Photoassisted Electrolysis of Water in Photoelectrochemical Cells. *Acc. Chem. Res.* **14**, 154-162.
- Hodes G, Ponash SJ, Heller A, Miller B (1985) Photoelectrochemical Cells Based on Polycrystalline Semiconductors. *Adv. in Electrochemistry and Electrochemical Engineering.* **13**, 113 - 158.
- Jaegermann W, Schmeisser D (1986) Reactivity of Layer Type Transition Metal Chalcogenides Towards Oxidation. *Surf. Sci.* **V165**, 143 - 160.
- Jakubowicz A, Mahalu D, Wolf M, Wold A, Tenne R (1989) WSe₂: Optical and electrical properties as related to surface passivation of recombination centers. *Phys. Rev. B* **40**, 2992 - 3000.
- Kautek W, Gobrecht J, Gerischer H (1980) The Applicability of Semiconducting Layered Materials for Electrochemical Solar Energy Conversion. *Ber. Bunsenges. Phys. Chem.* **84**, 1034 - 1040.
- Kam KK, Parkinson BA (1982) Detailed Photocurrent Spectroscopy of Semiconducting Group VI Transition Metal Dichalcogenides. *J. Phys. Chem.* **86**, 463 - 467.
- Lewerenz HJ, Heller A, Disalvo FJ (1980) Conversion Efficiency of WSe₂ Photoanodes. *J. Am. Chem. Soc.* **102**, 1877 - 1880.
- Lewerenz HJ, Ferris SD, Doherty CJ, Leamy HJ (1982) Charge Collection Microscopy on p-WSe₂: Recombination Sites and Minority Carrier Diffusion Length. *J. Electrochem. Soc.* **129**, 418 - 423.
- Mahalu D, Jakubowicz A, Wold A, Tenne R (1988) Passivation of Recombination Centers on the WSe₂ surface. *Phys. Rev. B* **38**, 1533 - 1535.
- Mahalu D, Peisach M, Jaegermann W, Wold A, Tenne R (1990) Controlled Photocorrosion of WSe₂: Influence of Molecular Oxygen. *J. Phys. Chem.* **94**, 8012 - 8013.
- Tributsch H (1978) Hole Reactions from d-Energy Bands of Layer Type Group VI Transition Metal Dichalcogenides: New Perspectives for Electrochemical Solar Energy Conversion. *J. Electrochem. Soc.* **125**, 1086 - 1093.
- Wilson J, Yoffe AD (1969) Transition Metal Dichalcogenides. *Adv. Phys.* **18**, 193 - 335.

Discussion with Reviewers

S.P. Shea: The authors have misinterpreted their EBIC data, which does not actually support their conclusion of enhanced current collection efficiency on $\parallel c$ facets of WSe₂. Consider their Fig. 5, for example. If the mechanism they propose is correct, then one would expect to see alternating bands of uniformly light and dark regions

corresponding to the $\parallel c$ and $\perp c$ facets, respectively. This is not what the pictures show. Instead, the left side of Fig. 5a shows an EBIC scan line which peaks at the bottom of each valley created by the intersection of adjacent facets, and which has a minimum at each ridge line between adjacent facets.

This is exactly what one would expect if the contrast were due to the interaction volume of the electron beam with the sample being of the same order as the features being examined. In this case the interaction volume would be entirely embedded in the sample when the beam entered the sample at the bottom of a valley, but would "bloom" out the sides of each facet when the beam was at the peak of a ridge. This is the same mechanism which limits the resolution of the EBIC technique in determining diffusion lengths in semiconductor diodes (see, e.g. Shea et al. 1978).

On the right side of Fig. 5a, the different orientation of the facets relative to the beam would mean that the EBIC signal would be minimal just to the right of one of the ridges, at the point where much of the beam would scatter out of the sample through the adjacent facet. Qualitatively these are exactly the effects seen in the figure. Fig. 4 also does not support the authors' conclusions, for similar reasons. Please comment.

Authors: The mechanism proposed by this reviewer (Shea et al. 1978) actually exists here. However, its contribution to the EBIC-signal at the steps is not substantial enough to explain the observed features of EBIC-profiles. Let us suppose that the reviewer is right, and there is no difference in the EBIC behavior of the $\parallel c$ and $\perp c$ facets. Then, for symmetrical position of the $\parallel c$ and $\perp c$ facets, all the effects suggested by the reviewer would be identical for these facets. Thus, EBIC-profiles for arbitrary facets of any kind should be identical, too. But this is not the case.

The magnification in Fig. 5 is not high enough to analyze an EBIC-profile within an individual step. Such an analysis, however, may be done for Fig. 6. One can see maxima of the EBIC-signal in the middle of the $\parallel c$ facets, and not at the bottom of valleys, as the reviewer proposes. On the contrary, for the $\perp c$ facets the EBIC-signal is always weaker in the middle and increases towards both edges (where the electron beam begins to hit the $\parallel c$ facets!). This regularity does not depend on the width of the facets.

Concerning the right side of Fig. 5 the reviewer's description fully agrees with our explanation given in the text. Actually, there is no sense in discussing the features of the EBIC image for this part of the etch pit. The $\parallel c$ facets were shadowed here during the gold evaporation (that was done at 45°-tilted position, see text). Therefore, there is no Schottky contact on these facets, and hence no EBIC (black contrast).

R. Matson: In reference to the severe electron beam damage to the sample, I assume 1) that the effect was monitored in the EBIC mode and 2) that the electron beam effects were greater with increased beam voltage and/or beam current, and slower scan rate (higher charge density per unit time). Do you have any idea why the electron beam effected the material in terms of its electrical properties (as measured by EBIC) in this manner? Did you observe a preferential degradation of the material's EBIC response at the $\parallel c$ edges? Did the material recover either with time or re-exposure to air (oxygen)? Is it possible that the electron beam is stimulating the desorption of oxygen or some other agent as a passivant?

Authors: We did not observe any preferential degradation of the material's EBIC response at the $\parallel c$ facets. Conversely, when the electron beam damage occurs (e.g. at room temperature), it is stronger at the $\perp c$ facets than at $\parallel c$ facets. Furthermore, the material did not recover neither with time nor with re-exposure to air at room temperature. The rest of the reviewer's assumptions are quite precise. This may indicate that the electron beam damage effects observed here are very similar to the phenomenon of electron-stimulated desorption (ESD) of oxygen, described in his own paper (Matson et al. 1988). Of course, we cannot totally exclude the presence of oxygen on WSe_2 etched surface - in spite of careful rinsing in hot KOH (see text) - since oxidation is one of the stages of the controlled anodic corrosion process. Therefore, the damage by ESD of oxygen is plausible. It should be emphasized that an oxide layer, if any, must be very thin, as it is not detected neither in TEM images nor in diffraction patterns (Fig. 3). Recent nuclear reaction analysis measurements using O^{18} (Mahalu et al. 1990, text reference) showed that a monolayer of oxide exists at the etched WSe_2 surface.

H.P. Strunk: Fig. 5: Where is the SE detector located in the image/sketch? This knowledge is necessary for the comparison of EBIC/SE images. Does the sketch in Fig. 5c compare in geometry/inclination to the micrographs in Figs. 5a and b?

The EBIC-contrast behavior of the steps seems to be very complicated: Fig. 4b shows dark/bright/dark contrasts, whereas Fig. 5b shows only dark/bright contrasts. In addition the contrasts in Figs. 5a and b are complementary, which suggests a purely topological explanation of the EBIC contrast. At sites with low SE-coefficients, i.e. comparatively high deposited energies in excitation volume (=dark in Fig. 5a), the EBIC-signal is high (=bright in Fig. 5b) because of a comparatively high charge carrier production in the excitation volume. How is this possibility of an artefact ruled-out?

R. Memming: Comparing Fig. 5a (SE) and 5b (EBIC) one can see an almost complementary contrast (besides the defect structures mentioned by the authors). Since

the contrast in the SE-image is due to topographical reasons this seems to be the same in the EBIC image (loss of electrons in the current signal).

Authors: Fig. 5: Regarding the geometry/inclination, the sketch at the bottom fully corresponds to the micrographs in Figs. 5a and b; the SE detector is located here to the left of the sample.

These indications explain already the SE-contrast of $\parallel c$ and $\perp c$ facets in Fig. 5a (left side). The $\perp c$ facets are tilted towards the SE detector, while the $\parallel c$ facets are tilted away from the detector; therefore, the $\parallel c$ facets appear dark on the SE image. Concerning EBIC, the orientation of various steps relative to the electron beam is most important for comparison of their current signals. One can see that, on the left side of the etch pit, the $\parallel c$ and $\perp c$ facets are oriented symmetrically to the electron beam. Hence, we interpret the enhanced EBIC-signal from $\parallel c$ facets as an intrinsic property of these facets, i.e. enhanced current collection efficiency compared to the $\perp c$ facets under the same conditions.

There is no artefact, i.e. there is no any physical relationship between SE- and EBIC-signals as H.P. Strunk assumes. The complementary nature of the SE- and EBIC-contrasts is only occasional. In other cases it might be different. See, for example, Fig. 4. The $\parallel c$ steps with enhanced EBIC-signal (Fig. 4b, arrowed) appear also with enhanced SE-signal (Fig. 4a), due to their appropriate orientation towards the SE detector. Note that the difference in the EBIC-contrast behavior of $\parallel c$ facets in Figs. 4b and 5b results from different orientation of the specimen relative to the electron beam (see text).

J.D. Meakin: There is unarguably a higher EBIC signal from the short $\parallel c$ steps than the longer $\perp c$ steps. However it is not clear that this is ascribable to enhanced current collection. There will be considerable elastic back scattering at the surface; electrons scattered from the short $\parallel c$ surfaces are much more likely to impact the surface again than electrons scattered from the long $\perp c$ surfaces. Can the authors exclude an enhanced EBIC deriving from this effect?

Authors: The reviewer is absolutely right regarding this mechanism of an EBIC enhancement. It cannot be totally excluded. In the present case, however, the contribution of this mechanism should not be prominent. If the EBIC enhancement were deriving from this effect only, the EBIC signal on a $\parallel c$ step would be minimal on the top of this step (maximum distance from the neighboring $\perp c$ step) and maximal at the bottom of the same step (minimal distance from the neighboring $\perp c$ step). Let us consider now Fig. 6, where the high magnification allows to resolve reliably the EBIC profile along the $\parallel c$ steps. One can clearly see maxima of the EBIC signal located always in the middle of $\parallel c$ steps. Further-

more, Fig. 6 shows the weaker EBIC signal from the $\perp c$ steps, even when they are shorter than the neighboring $\parallel c$ steps. These findings support our conclusion of an enhanced current collection from $\parallel c$ steps.

J.D. Meakin: Could you give some estimate of the hole diffusion distance which is presumably the carrier responsible for EBIC in the n-type WSe₂?

Authors: The minority carrier diffusion length (L) was not measured in this work. Previous measurements show L to be ca. 3.5 μm in the n-type WSe₂ (Jakubowicz et al. 1989, text reference), and ca. 1.5 μm in the p-type WSe₂ (Lewerenz et al. 1982, text reference).

H.P. Strunk: Fig. 7b: The discussed areas with strong dark contrast look very like sites of charging (low temperature and thus possibly low conductivity of the semiconductor in regions where by geometry the cross-section of the current path is small). Please comment.

Authors: The presence of a gold layer (Schottky contact) that is grounded via current amplifier prevents any surface charging. Hence, the charged regions assumed by the reviewer should be located in a near-surface layer of the bulk. In that case they are most probably associated with crystal defects of some kind. Hence, our explanation is very close to the reviewer's assumption. We also need to add that such areas of reduced EBIC signal on the $\parallel c$ steps appear, as a rule, only at the initial stages of the CAC process.

H.P. Strunk: Imaging of surface steps in TEM generally requires specifically selected excitation conditions. What are the contrast mechanisms operative in Fig. 3a?

Authors: We did not select specific conditions for imaging these low steps by TEM. It follows from our observations that in this case the image contrast is not of a diffraction origin. A decoration of low surface steps with heavy W atoms cannot be excluded.

J.D. Meakin: What is the origin of the ring pattern on Fig. 3b? Is it from surface corrosion?

Authors: The appearance of two rings seen in Fig. 3b does not result from any surface corrosion. These are actually the first and second Laue zones, respectively.

Additional References

Matson R, Kazmerski LL, Noufi R, Cahen D. (1988) Electron stimulated desorption of oxygen from, and subsequent type conversion of, thin-film p-CuInSe₂. *J. Vac. Sci. Technol. A* 7, 230 - 233.

Shea SP, Partain LD, Warter PJ (1978) Resolution limits of the EBIC technique in the determination of diffusion length in semiconductors. *Scanning Electron Microsc.* 1978; I: 435 - 444.